GEOLOGY | THE GEOLOGICAL SOCIETY OF AMERICA®

https://doi.org/10.1130/G45868.1

Manuscript received 29 November 2018
Revised manuscript received 10 May 2019
Manuscript accepted 14 May 2019



Published online 31 May 2019

# From fault creep to slow and fast earthquakes in carbonates

François X. Passelègue[1,2], Jérôme Aubry[3], Aurélien Nicolas[3], Michele Fondriest[2], Damien Deldicque[3], Alexandre Schubnel[3], and Giulio Di Toro[2,4]

[1]Laboratory of Experimental Rock Mechanics, École Polytechnique Fédérale de Lausanne, 1015 Lausanne, Switzerland
[2]School of Earth and Environmental Sciences, The University of Manchester, Manchester M13 9QQ, UK
[3]UMR8538, Ecole Normale Supérieure, 75231 Paris Cedex 5, France
[4]Dipartimento di Geoscienze, Università degli Studi di Padova, 35131 Padua, Italy

## ABSTRACT

**A major part of the seismicity striking the Mediterranean area and other regions worldwide is hosted in carbonate rocks. Recent examples are the destructive earthquakes of L'Aquila ($M_w$ 6.1) in 2009 and Norcia ($M_w$ 6.5) in 2016 in central Italy. Surprisingly, within this region, fast (≈3 km/s) and destructive seismic ruptures coexist with slow (≤10 m/s) and nondestructive rupture phenomena. Despite its relevance for seismic hazard studies, the transition from fault creep to slow and fast seismic rupture propagation is still poorly constrained by seismological and laboratory observations. Here, we reproduced in the laboratory the complete spectrum of natural faulting on samples of dolostones representative of the seismogenic layer in the region. The transitions from fault creep to slow ruptures and from slow to fast ruptures were obtained by increasing both confining pressure ($P$) and temperature ($T$) up to conditions encountered at 3–5 km depth (i.e., $P$ = 100 MPa and $T$ = 100 °C), which corresponds to the hypocentral location of slow earthquake swarms and the onset of seismicity in central Italy. The transition from slow to fast rupture is explained by an increase in the ambient temperature, which enhances the elastic loading stiffness of the fault, i.e., the slip velocities during nucleation, allowing flash weakening and, in turn, the propagation of fast ruptures radiating intense high-frequency seismic waves.**

## INTRODUCTION

In Earth's upper crust, faults release elastic strain energy stored in the wall rocks via different modes of slip. Depending on the velocity of the rupture front ($V_r$), faults may creep or generate slow ($V_r \leq 10$ m/s; Ide et al., 2007), sub-Rayleigh ($V_r \approx 3000$ m/s; also called fast ruptures), or supershear ($V_r \geq 4200$ m/s) earthquakes (Kanamori and Brodsky, 2004; Bouchon and Vallée, 2003; Passelègue et al., 2013; Marty et al., 2019). The Mediterranean area and several other regions worldwide are affected by moderate- to large-magnitude earthquakes (Chiaraluce, 2012; Valoroso et al., 2013) nucleating and propagating within (4–8 km) carbonate sequences (i.e., limestones and dolostones). This is the case of the Northern and Central Apennines of Italy, which were recently struck by destructive seismic sequences largely hosted within dolomitic rocks (Figs. 1A and 1B; Chiaraluce, 2012; Valoroso et al., 2013). These sequences were characterized by complex spatio-temporal distributions of mainshocks-aftershocks, with (1) most of the seismicity compartmentalized between 10 km and ~3 km depth, and (2) a sharp upper seismicity cutoff at ~3 km depth (Fig. 1B; Chiaraluce, 2012; Valoroso et al., 2013). Remarkably, in this region, destructive fast seismic ruptures coexist with slow (≤10 m/s) and nondestructive rupture phenomena (Figs. 1A and 1B; Crescentini et al., 1999; Amoruso et al., 2002). From a rock mechanics point of view, the coexistence of these different modes of slip remains enigmatic because carbonates can accommodate deformation by crystal-plastic processes, such as aseismic mechanical twinning and dislocation glide, even at room temperature (De Bresser and Spiers, 1997). The ability of calcite crystals to deform plastically at low pressure ($P$) and temperature ($T$) can explain the lack of acoustic emission activity (microseismicity) during failure of carbonates at shallow depth conditions (Schubnel et al., 2006; Nicolas et al., 2017). To investigate the frictional stability of carbonates, recent experimental studies focused on the frictional behavior of calcite- and dolomite-rich fault rocks sheared at subseismic to seismic slip rates to determine the frictional behavior of carbonates at ambient and crustal temperatures (Verberne et al., 2015; Fondriest et al., 2013; De Paola et al., 2015). Here, we report the results of triaxial experiments (see the method in the GSA Data Repository[1]) performed on saw-cut samples cored in dolostone blocks of the Mendola Formation (northeast Italy, Upper Triassic in age) (Fondriest et al., 2015).

## METHODS

The experiments were conducted in ambient conditions (temperature and pressure) typical of Earth's crust where all these different slip modes occur (Fig. 1). We studied the influence of both confining pressure and bulk temperature on the stability of the experimental fault system. Experiments were coupled to strain gauges and an acoustic sensor array to discriminate the nature of the seismicity (see detailed methods in the Data Repository).

## EXPERIMENTAL RESULTS

At 25 °C, slip initiated when the shear stress reached the peak strength of the fault, corresponding to a static friction, $f_s$, = $\tau_0/\sigma_n^0 \approx 0.4$ (where $\tau_0$ and $\sigma_n^0$ are the shear stress and the normal stress at the onset of instability, respectively). At this temperature, the fault exhibited typical frictional behavior (dependence of peak shear stress on confining pressure), and strain energy accumulated during loading was released by stable slip (Fig. 1C). Increasing the ambient temperature to 65 °C preserved the frictional behavior of the fault but led to a transition from stable slip to stick-slip motion (Fig. 1D). In this case, while stress-strain curves suggest stick-slip motion, slow ruptures of ~0.1 m/s were observed, and no high-frequency radiations were recorded. At 100 °C, the fault exhibited a different mechanical behavior. Fast ruptures

[1]GSA Data Repository item 2019267, detailed methods and supplementary microstructural and mechanical results, is available online at http://www.geosociety.org/datarepository/2019/, or on request from editing@geosociety.org.

CITATION: Passelègue, F.X., et al., 2019, From fault creep to slow and fast earthquakes in carbonates: Geology, v. 47, p. 744–748, https://doi.org/10.1130/G45868.1

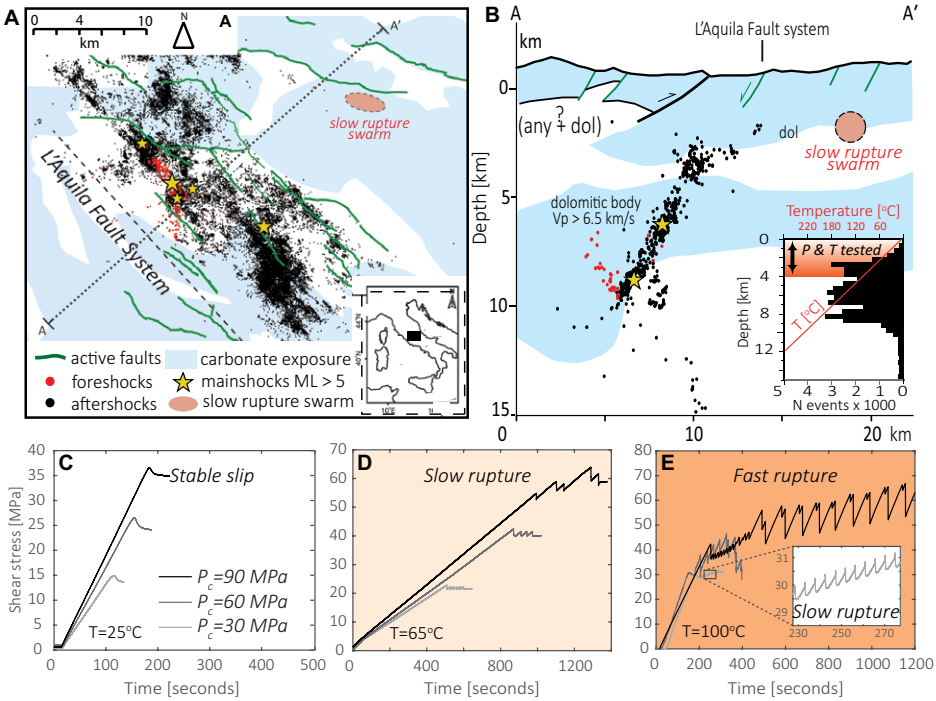


**Figure 1. A: Geographical distribution of seismicity of L'Aquila (central Italy) 2009 earthquake sequence (Valoroso et al., 2013). Surface exposure of carbonate rocks is from published geological maps (Ghisetti and Vezzani, 1998). Approximate location of slow rupture swarm is derived from geodetic studies (Crescentini et al., 1999; Amoruso et al., 2002). B: Cross section of L'Aquila fault system (A-A′ in A; Ghisetti and Vezzani, 1998; Valoroso et al., 2013). Dolostone body is interpreted from seismic tomography (Di Stefano et al., 2011) and aeromagnetic anomaly measurements (Speranza and Minelli, 2014). Inset in B displays distribution with depth of seismicity associated with the L'Aquila 2009 sequence (Valoroso et al., 2013). Red line represents the evolution of temperature within the crust assuming a geothermal gradient of 25 °C/km. Background orange-colored area highlights temperature (*T*) and pressure (*P*) conditions tested in experiments of this study. C–E: Results of experiments conducted at increasing confining pressures (30, 60, and 90 MPa) and temperatures (25, 65, and 100 °C).**

were observed at both 60 and 90 MPa confining pressure, while only slow ruptures were observed at 30 MPa confining pressure. Fast ruptures induced strong high-frequency motions, recorded on both high-frequency acoustic and dynamic strain monitoring systems. Note that coexisting slow ruptures, which do not produce high-frequency motions, were also observed in the first stage of the experiments conducted at 90 MPa confining pressure. For each event, the peak shear stress at the onset of slip increased with normal stress, which shows that fault reactivation respects frictional criteria independent of the temperature and pressure conditions (Fig. 2A).

At low confining pressure (30 MPa), the increase of the peak friction with ambient temperature led to a transition from stable slip to slow rupture. At 60 and 90 MPa confining pressure, a similar trend was observed: An increase in temperature led to an increase of the peak friction coefficient and to a transition from stable slip to slow rupture, but to fast rupture at $T$ = 100 °C (Fig. 2A). Moreover, the amount of stress released via the different modes of slip observed depended on the peak shear stress reached during the loading. Larger peak shear stress led to larger stress drop (Fig. 2B). However, frictional drop remained small during stable slip and slow rupture ($\Delta f \approx 0.05$). For similar values of initial shear stress, fast rupture released a larger amount of shear stress (Fig. 2B), i.e., larger frictional drop, which ranged from 0.07 to 0.22 (Fig. 2B). This behavior is highlighted by comparing the static stress drop of each event to the related amount of slip. Each mode of slip (i.e., stable, slow and fast rupture) presents a different linear relation between the static stress drop and the fault slip (Fig. 2C). For the same value of slip, the resulting stress drop is larger during fast ruptures than during slow ruptures. Note that slow ruptures observed at both 65 °C and 100 °C followed the same trend, suggesting similar mechanisms. These results suggest that fast ruptures are more dispersive than slow ruptures.

## NUCLEATION OF SLOW AND FAST RUPTURES

Using the travel times of the rupture front recorded by the array of strain gauges located along fault strike, estimates for $V_r$ during slow rupture propagation range from 0.1 to 20 m/s (Fig. 3A). These values are in agreement with rupture velocities of natural slow earthquakes (Ide et al., 2007), suggesting that our experimental slow ruptures are similar to those observed in nature. An increase of $V_r$ during rupture propagation was observed along fault strike (Fig. 3A). In addition, increasing the initial shear stress (i.e., the confining pressure) led to larger rupture velocities at the onset of the frictional instability. To further analyze the influence of

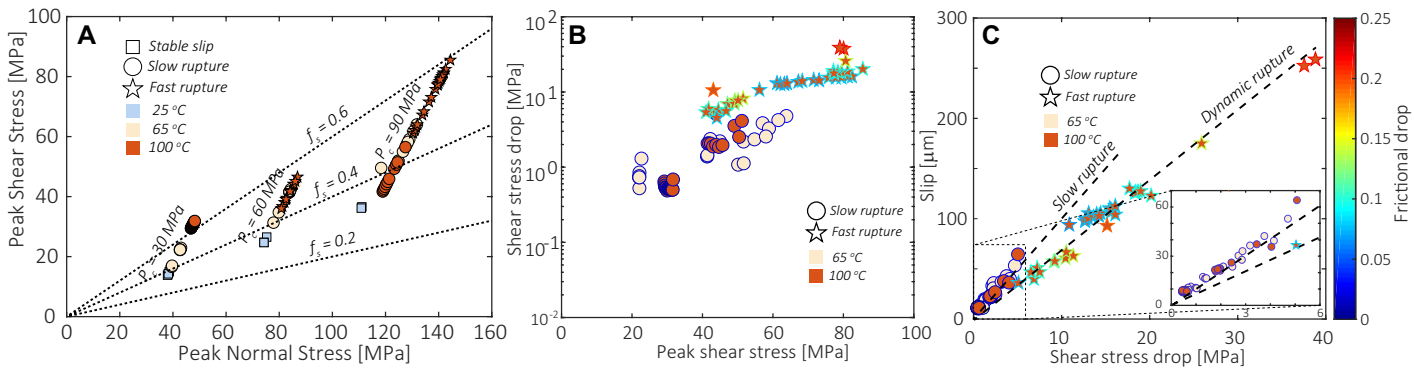


**Figure 2. A: State of stress (shear stress and normal stress) at onset of slip for each experimental event. Black dashed lines correspond to different values of friction coefficient. B: Static shear stress drop as a function of initial peak shear stress. C: Scaling law of seismic slip versus static stress drop for each mode of slip. Black dashed lines correspond to best linear fit of each mode of slip. Color bar refers to the rim of each symbol in B and C, and indicates frictional drop during each slip event.**

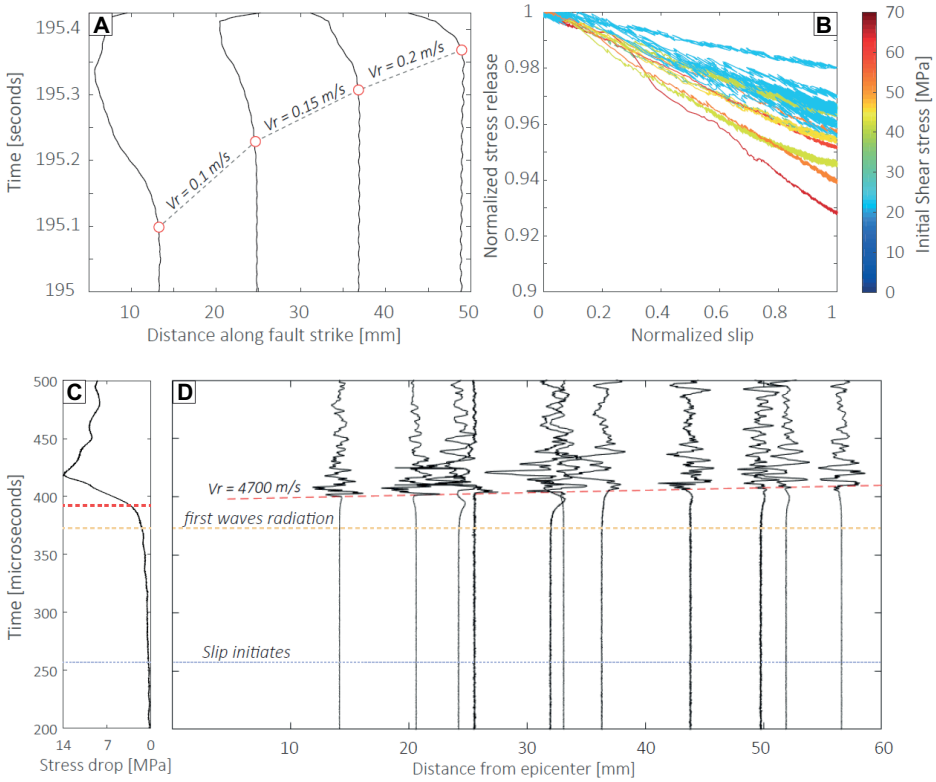


**Figure 3. A: Evolution of strain on each strain gauge (located along fault strike) as a function of time. Initiation of strain drop (red circles) on each strain gauge was used to track rupture-front velocity between each strain gauge. B: Evolution of shear stress versus slip during all slow rupture events. Slip was normalized by the final slip of each event, and shear stress was normalized by the peak shear stress at the onset of slip (color bar). C: Evolution of stress during nucleation and propagation of fast rupture. D: Evolution of acoustic signals during nucleation and propagation of fast rupture as a function of distance from initiation of high-frequency motions. Alignment of the high-frequency radiation front allowed us to estimate the rupture velocity during a slip event.**

the background shear stress, we computed the evolution of stress with slip (weakening stiffness $K = \Delta\tau/\Delta u$, where $u$ corresponds to the slip along the fault) during each event induced during the experiments conducted at 65 °C under 30, 60, and 90 MPa confining pressure, respectively. The weakening process during slow rupture was slip weakening (Fig. 3B), confirming recent expectations (Ikari et al., 2013). In addition, the increase in the peak shear stress along fault strike led to a larger fraction of shear stress released during the slip events (Fig. 3B). Assuming a typical earthquake energy budget (Kanamori and Brodsky, 2004), pure slip weakening behavior is expected to drastically limit the radiated energy during rupture propagation, explaining the smaller stress drop for a given amount of slip compared to fast rupture phenomena.

Fast earthquakes present a complex nucleation behavior. At the onset of slip, dynamic strain recording showed that fault slip accelerates and radiates low-amplitude and relatively low-frequency (20 kHz) acoustic waves (Fig. 3C). At a critical point (red dashed line in Fig. 3C), the shear stress drops abruptly within 20 µs, initiating high-frequency wave radiation. Using piezoelectric transducers as seismic rupture chronometers (Passelègue et al., 2016), we estimated rupture velocities ranging from 1500 to 5200 m/s. Our estimations for ruptures speed are compatible with previous studies (Passelègue et al., 2016) and with the rupture speed of classic earthquakes (Ide et al., 2007). The amplitude and the frequency of the acoustic motions increased with the stress release rate (Figs. 3C and 3D). Note that the radiation of the high-frequency wave front appeared to occur after the release of half of the shear stress (half of the dynamic stress drop). These results suggest that fault weakening initiates before the radiation of high-frequency waves.

## POSTMORTEM MICROSTRUCTURES

Fault surfaces recovered from experiments where stable slip and slow ruptures occurred have highly light-reflective patches visible to the naked eye. These patches are similar to the mirror-like slip surfaces previously observed in nature or after friction experiments conducted with subseismic to seismic slip rates on carbonate rock gouges (Fondriest et al., 2013; Verberne et al., 2015). Scanning electron microscope images reveal the extremely smooth topography of mirror surfaces, composed of tightly packed to welded, subrounded nanograins with negligible porosity (Fig. 4A). In contrast, fault surfaces that experienced fast ruptures are on average much rougher than those after stable slip and slow rupture and are pervasively covered by a foam-like material embedding small well-rounded nanograins with an average size of 150 nm (Fig. 4B). The foam-like material locally includes ultrathin (>5 nm in thickness) filaments and patches connecting and wrapping the nanograins (Fig. 4B), recalling frictional melting textures found in silicate-bearing rocks sheared under similar deformation conditions (Passelègue et al., 2016).

## INTERPRETATION AND DISCUSSION

Our experiments reproduced the complete spectrum of natural faulting: (1) stable slip at room temperature, (2) slow ruptures at 65 °C, and (3) coexisting slow and fast ruptures at 100 °C. Our experimental approach succeeded in explaining the onset of fault creep and the transition from slow ruptures (Crescentini et al., 1999; Amoruso et al., 2002) to typical seismicity at *P-T* conditions encountered at 3 km depth, as observed in the Central Apennines based on seismological and geodetic investigations (Chiaraluce, 2012). It seems that this first-order similarity between experimental and natural fault-slip modes was mainly controlled by the variation in temperature. However, since all the experiments were performed in dry conditions, we cannot rule out the potential role played by pore fluids.

In our experiments, the transition from stable to unstable slip was promoted by a combination of the confining pressure, which increases the stiffness of the fault (Fig. DR2 in the Data Repository; Leeman et al., 2016), and the fault temperature, which promotes unstable behavior of rocks and carbonates (Blanpied et al., 1995; Brantut et al., 2011; Verberne et al., 2015; Pluymakers et al., 2016). This finding could be counterintuitive, since an increase in ambient pressure and temperature enhances microplasticity in carbonates, which should release part of the stored elastic strain energy and reduce the rupture speed (Rutter, 1972; Nicolas et al., 2017). In our experiments, the stiffness of the fault increased with both bulk temperature and confining pressure (see the Data Repository, and Fig. DR2a therein) and became greater than the stiffness of the apparatus (Fig. DR2; Fig. 4C), reducing the nucleation length to sizes smaller than the experimental fault length (Fig. 4C). These processes are at the origin of the transition from a stable to slow rupture front.

The transition from slow to fast rupture is more complicated. First, the transition seems to depend on the peak friction along the fault at the onset of slip (Fig. 2A), as previously observed (Ben-David et al., 2010; Passelègue et al., 2013). However, large values of peak friction alone are

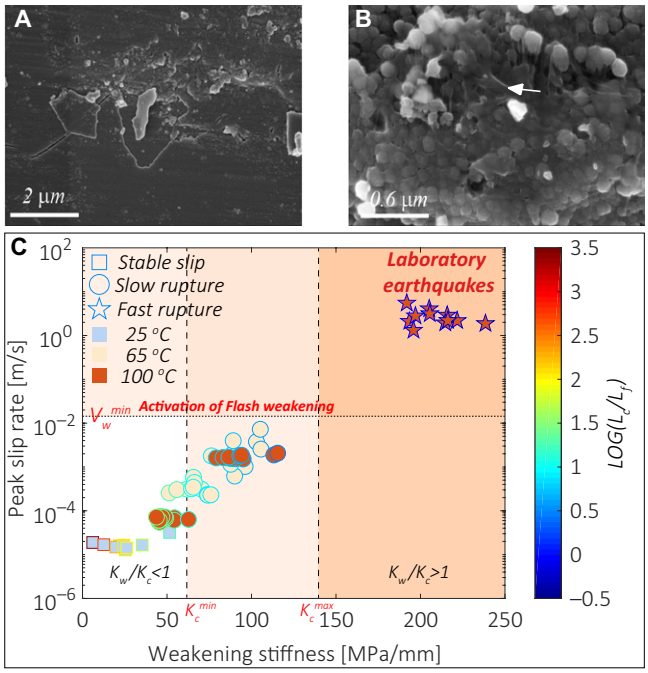


**Figure 4. A–B: Scanning electron microscope (SEM) images of fault surfaces that were associated with slow and fast propagating ruptures, respectively. White arrow in B highlights location of foam-like material. C: Peak slip rate versus weakening stiffness ($K_w$) during each event. $K_c^{min}$ and $K_c^{max}$ define minimum and maximum stiffness of experimental apparatus, respectively. $V_w$ is minimal velocity required to trigger flash heating and weakening phenomena at 100 °C ambient temperature, assuming the relation $V_w = \{[\rho \times C_p]^2[T_w - T_0]^2\pi \times \kappa/[D(\tau_c)^2]\}$, where $\rho$ is rock density (2650 kg/m³), $C_p$ is heat capacity (900 J kg$^{-1}$ K$^{-1}$), $\kappa$ is thermal diffusivity (1.25 × 10$^{-6}$ m² s$^{-1}$), $T_w$ is decarbonation temperature (600 °C), $T_0$ is ambient temperature, $D$ is asperity size (50 and 1 μm), and $\tau_c$ is contact hardness of dolomite (3 GPa; Goldsby and Tullis, 2011). Color bar corresponds to nucleation length of each event normalized by fault length ($L_f$). Nucleation length was calculated following $L_c = (2\beta \times \mu \times G)/[\tau_0 \times (1 - f_d/f_s)^2]$ (Campillo and Ionescu, 1997), where β is nondimensional shape factor coefficient (≈1.158), μ is shear modulus of dolomite estimated using strain measurements, and $G$ is effective fracture energy, $G = u \times \sigma_n \times (f_s - f_d)/2$. $\tau_0$ and $\sigma_n$ are the peak shear stress and the normal stress at the instability, respectively. $f_s$ and $f_d$ are the static and the dynamic friction coefficient, respectively.**

not sufficient to induce fast rupture propagation at low confining pressure. As expected theoretically, ruptures speed increases with the fault weakening rate. In our experiments, the weakening rate increased with the peak slip rate reached during rupture propagation (Fig. 4C). For weakening stiffness ($K$) above that of the apparatus ($K > K_c$), the slip rate became faster than 1 m/s, and could reach up to 10 m/s, within the limit of our resolution (see the Data Repository). This enhancement in the weakening stiffness and weakening rate can be explained by the activation of weakening mechanisms due the increase in the slip rates.

While the activation of plastic mechanisms explains the weakening and transition from stable to unstable behavior in calcite (De Paola et al., 2015; Green et al., 2015; Verberne et al., 2015, 2017; Pozzi et al., 2018), these mechanisms are not dominant in dolomite (see the Data Repository). However, sliding velocities above a critical weakening velocity ($V_w$) are expected to activate flash heating phenomena during fast events (Goldsby and Tullis, 2011; Passelègue et al., 2014; Aubry et al., 2018). First, based on the size of initial asperities, flash decarbonation is expected to occur when the slip rate becomes larger than 1 cm/s (Fig. 4C), explaining the low weakening observed during slow ruptures ($10^{-4} < V_s^{slow} < 10^{-2}$ m/s). Second, assuming the average slip rate observed during fast ruptures (≈2.5 m/s), we can state that asperities larger than 0.24 μm are expected to decarbonate during their lifetimes during fast ruptures (see the Data Repository). These results agree with postmortem microstructures, which highlighted nanograins wrapped by a foam-like material that resembles a solidified melt. Note that in carbonate minerals, the melting point decreases dramatically in the presence of $CO_2$ at room humidity conditions and can be close to the decarbonation temperature, explaining the melting observed at the scale of the asperities (Wyllie, 1965). The activation of flash heating on asperities during instabilities seems to explain both (1) the gap existing between slow and fast ruptures in terms of weakening and slip velocity (Fig. 4C), and (2) the strong enhancement of the weakening rate during the nucleation of fast ruptures, which initiates the radiation of high-frequency seismic waves (Figs. 3C and 3D).

To conclude, our results demonstrate that, in contrast to silicate rocks such as granite, which behave dynamically (fast rupture propagation) without activation of strong weakening processes (Blanpied et al., 1995; Passelègue et al., 2016; Leeman et al., 2016), dynamic rupture and high-frequency radiation require the activation of intense fault weakening in carbonates, such as frictional flash weakening in dolomite or plastic processes in calcite (Verberne et al., 2015, 2017; Pluymakers et al., 2016; Pozzi et al., 2018).


## ACKNOWLEDGMENTS

Passelègue acknowledges funding provided by the Swiss National Science Foundation through grant PZENP2/173613. This work was funded by the European Research Council through grant NE/K009656/1 to Di Toro and through grant 681346 to Schubnel. We thank Experimental Officer Yves Pinquier for assistance with specimen fabrication and equipment maintenance. We acknowledge A. Niemeijer, M. Ikari, and N. De Paola for their reviews, which improved the paper significantly.


## REFERENCES CITED


Amoruso, A., Crescentini, L., Morelli, A., and Scarpa, R., 2002, Slow rupture of an aseismic fault in a seismogenic region of central Italy: Geophysical Research Letters, v. 29, p. 72-1–72-4, https://doi.org/10.1029/2002GL016027.

Aubry, J., Passelègue, F.X., Deldicque, D., Girault, F., Marty, S., Lahfid, A., et al., 2018, Frictional heating processes and energy budget during laboratory earthquakes: Geophysical Research Letters, v. 45, p. 12,274–12,282, https://doi.org/10.1029/2018GL079263.

Ben-David, O., Cohen, G., and Fineberg, J., 2010, The dynamics of the onset of frictional slip: Science, v. 330, p. 211–214, https://doi.org/10.1126/science.1194777.

Blanpied, M.L., Lockner, D.A., and Byerlee, J.D., 1995, Frictional slip of granite at hydrothermal conditions: Journal of Geophysical Research–Solid Earth, v. 100, no. B7, p. 13,045–13,064, https://doi.org/10.1029/95JB00862.

Bouchon, M., and Vallée, M., 2003, Observation of long supershear rupture during the magnitude 8.1 Kunlunshan earthquake: Science, v. 301, p. 824–826.

Brantut, N., Schubnel, A., and Guéguen, Y., 2011, Damage and rupture dynamics at the brittle-ductile transition: The case of gypsum: Journal of Geophysical Research–Solid Earth, v. 116, no. B1, B01404, https://doi.org/10.1029/2010JB007675.

Campillo, M., and Ionescu, I.R., 1997, Initiation of antiplane shear instability under slip dependent friction: Journal of Geophysical Research–Solid Earth, v. 102, no. B9, p. 20,363–20,371.

Chiaraluce, L., 2012, Unravelling the complexity of Apenninic extensional fault systems: A review of the 2009 L'Aquila earthquake (Central Apennines, Italy): Journal of Structural Geology, v. 42, p. 2–18, https://doi.org/10.1016/j.jsg.2012.06.007.

Crescentini, L., Amoruso, A., and Scarpa, R., 1999, Constraints on slow earthquake dynamics from a swarm in central Italy: Science, v. 286, p. 2132–2134, https://doi.org/10.1126/science.286.5447.2132.

De Bresser, J.H.P., and Spiers, C.J., 1997, Strength characteristics of the r, f, and c slip systems in calcite: Tectonophysics, v. 272, p. 1–23, https://doi.org/10.1016/S0040-1951(96)00273-9.

De Paola, N., Holdsworth, R.E., Viti, C., Collettini, C., and Bullock, R., 2015, Can grain size sensitive flow lubricate faults during the initial stages of earthquake propagation?: Earth and Planetary Science Letters, v. 431, p. 48–58, https://doi.org/10.1016/j.epsl.2015.09.002.

Di Stefano, R., Chiarabba, C., Chiaraluce, L., Cocco, M., De Gori, P., Piccinini, D., and Valoroso, L., 2011, Fault zone properties affecting the rupture evolution of the 2009 (Mw 6.1) L'Aquila earthquake (central Italy): Insights from seismic tomography: Geophysical Research Letters, v. 38, L10310, https://doi.org/10.1029/2011GL047365.

Fondriest, M., Smith, S.A., Candela, T., Nielsen, S.B., Mair, K., and Di Toro, G., 2013, Mirror-like faults and power dissipation during earthquakes:

Geology, v. 41, p. 1175–1178, https://doi.org/10.1130/G34641.1.
Fondriest, M., Aretusini, S., Di Toro, G., and Smith, S.A., 2015, Fracturing and rock pulverization along an exhumed seismogenic fault zone in dolostones: The Foiana fault zone (southern Alps, Italy): Tectonophysics, v. 654, p. 56–74, https://doi.org/10.1016/j.tecto.2015.04.015.
Ghisetti, F., and Vezzani, L., 1998, Segmentation and tectonic evolution of the Abruzzi-Molise thrust belt (Central Apennines, Italy): Annales Tectonicae, v. 12, p. 97–112.
Goldsby, D.L., and Tullis, T.E., 2011, Flash heating leads to low frictional strength of crustal rocks at earthquake slip rates: Science, v. 334, p. 216–218, https://doi.org/10.1126/science.1207902.
Green, H.W., II, Shi, F., Bozhilov, K., Xia, G., and Reches, A.Z., 2015, Phase transformation and nanometric flow cause extreme weakening during fault slip: Nature Geoscience, v. 8, p. 484–489, https://doi.org/10.1038/ngeo2436.
Ide, S., Beroza, G.C., Shelly, D.R., and Uchide, T., 2007, A scaling law for slow earthquakes: Nature, v. 447, p. 76–79, https://doi.org/10.1038/nature05780.
Ikari, M.J., Marone, C., Saffer, D.M., and Kopf, A.J., 2013, Slip weakening as a mechanism for slow earthquakes: Nature Geoscience, v. 6, p. 468–472, https://doi.org/10.1038/ngeo1818.
Kanamori, H., and Brodsky, E.E., 2004, The physics of earthquakes: Reports on Progress in Physics, v. 67, no. 8, p. 1429–1496, https://doi.org/10.1088/0034-4885/67/8/R03.
Leeman, J.R., Saffer, D.M., Scuderi, M.M., and Marone, C., 2016, Laboratory observations of slow earthquakes and the spectrum of tectonic fault slip modes: Nature Communications, v. 7, p. 11104, https://doi.org/10.1038/ncomms11104.
Marty, S., Passelègue, F.X., Aubry, J., Bhat, H.S., Schubnel, A., and Madariaga, R., 2019, Origin of high-frequency radiation during laboratory earthquakes: Geophysical Research Letters, v. 46, no. 7, p. 3755–3763, https://doi.org/10.1029/2018GL080519.
Nicolas, A., Fortin, J., Regnet, J.B., Verberne, B.A., Plümper, O., Dimanov, A., et al., 2017, Brittle and semibrittle creep of Tavel limestone deformed at room temperature: Journal of Geophysical Research–Solid Earth, v. 122, p. 4436–4459, https://doi.org/10.1002/2016JB013557.
Passelègue, F.X., Schubnel, A., Nielsen, S., Bhat, H.S., and Madariaga, R., 2013, From sub-Rayleigh to supershear ruptures during stick-slip experiments on crustal rocks: Science, v. 340, p. 1208–1211, https://doi.org/10.1126/science.1235637.
Passelègue, F.X., Goldsby, D.L., and Fabbri, O., 2014, The influence of ambient fault temperature on flash-heating phenomena: Geophysical Research Letters, v. 41, p. 828–835, https://doi.org/10.1002/2013GL058374.
Passelègue, F., Schubnel, A., Nielsen, S., Bhat, H.S., Deldicque, D., and Madariaga, R., 2016, Dynamic rupture processes inferred from laboratory microearthquakes: Journal of Geophysical Research–Solid Earth, v. 121, p. 4343–4365, https://doi.org/10.1002/2015JB012694.
Pluymakers, A.M.H., Niemeijer, A.R., and Spiers, C.J., 2016, Frictional properties of simulated anhydrite-dolomite fault gouge and implications for seismogenic potential: Journal of Structural Geology, v. 84, p. 31–46, https://doi.org/10.1016/j.jsg.2015.11.008.
Pozzi, G., De Paola, N., Nielsen, S.B., Holdsworth, R.E., and Bowen, L., 2018, A new interpretation for the nature and significance of mirror-like surfaces in experimental carbonate-hosted seismic faults: Geology, v. 46, p. 583–586, https://doi.org/10.1130/G40197.1.
Rutter, E.H., 1972, The influence of interstitial water on the rheological behaviour of calcite rocks: Tectonophysics, v. 14, p. 13–33, https://doi.org/10.1016/0040-1951(72)90003-0.
Schubnel, A., Walker, E., Thompson, B.D., Fortin, J., Guéguen, Y., and Young, R.P., 2006, Transient creep, aseismic damage and slow failure in Carrara marble deformed across the brittle-ductile transition: Geophysical Research Letters, v. 33, L17301, https://doi.org/10.1029/2006GL026619.
Speranza, F., and Minelli, L., 2014, Ultra-thick Triassic dolomites control the rupture behavior of the Central Apennine seismicity: Evidence from magnetic modeling of the L'Aquila fault zone: Journal of Geophysical Research–Solid Earth, v. 119, p. 6756–6770, https://doi.org/10.1002/2014JB011199.
Valoroso, L., Chiaraluce, L., Piccinini, D., Di Stefano, R., Schaff, D., and Waldhauser, F., 2013, Radiography of a normal fault system by 64,000 high-precision earthquake locations: The 2009 L'Aquila (central Italy) case study: Journal of Geophysical Research–Solid Earth, v. 118, p. 1156–1176, https://doi.org/10.1002/jgrb.50130.
Verberne, B.A., Niemeijer, A.R., De Bresser, J.H., and Spiers, C.J., 2015, Mechanical behavior and microstructure of simulated calcite fault gouge sheared at 20–600 C: Implications for natural faults in limestones: Journal of Geophysical Research–Solid Earth, v. 120, p. 8169–8196, https://doi.org/10.1002/2015JB012292.
Verberne, B.A., Chen, J., Niemeijer, A.R., Bresser, J.H., Pennock, G.M., Drury, M.R., and Spiers, C.J., 2017, Microscale cavitation as a mechanism for nucleating earthquakes at the base of the seismogenic zone: Nature Communications, v. 8, p. 1645, https://doi.org/10.1038/s41467-017-01843-3.
Wyllie, P.J., 1965, Melting relationships in the system $CaO$-$MgO$-$CO_2$–$H_2O$, with petrological applications: Journal of Petrology, v. 6, p. 101–123, https://doi.org/10.1093/petrology/6.1.101.

Printed in USA